GEOPHYSICS

Role of warm subduction in the seismological properties of the forearc mantle: An example from southwest Japan

Changyeol Lee[1] and YoungHee Kim[2]*

A warm slab thermal structure plays an important role in controlling seismic properties of the slab and mantle wedge. Among warm subduction zones, most notably in southwest Japan, the spatial distribution of large *S*-wave delay times and deep nonvolcanic tremors in the forearc mantle indicate the presence of a serpentinite layer along the slab interface. However, the conditions under which such a layer is generated remains unclear. Using numerical models, we here show that a serpentinite layer begins to develop by the slab-derived fluids below the deeper end of the slab-mantle decoupling interface and grows toward the corner of the mantle wedge along the interface under warm subduction conditions only, explaining the large *S*-wave delay times in the forearc mantle. The serpentinite layer then allows continuous free-fluid flow toward the corner of the mantle wedge, presenting possible mechanisms for the deep nonvolcanic tremors in the forearc mantle.

INTRODUCTION

Upon subduction, fluids are released from the subducting slab through a series of metamorphic reactions, and the increased fluid flux into the mantle wedge modifies its chemical and physical properties. This subduction-related dehydration and hydration play critical roles in controlling seismic parameters (seismic velocities and anisotropies) of the descending slab and overlying mantle wedge, as evidenced in a number of subduction zones (*1*, *2*). Among various subduction zones, the Japan subduction zone shows the clearest along-arc variations in seismic properties and processes, mainly dictated by the thermal structure of the slab. In particular, thermal-petrologic models (*3*) predict differences in seismicity and seismic structure in southwest and northeast Japan. The warm subduction conditions in southwest Japan result in the sub-forearc transformation of hydrated metabasalt to eclogite and its subarc partial melting, consistent with the depth extent of the seismic low-velocity layer and intermediate-depth intraslab earthquakes (*4*–*6*) and the Quaternary arc adakites in Sambe and Daisen arc volcanoes (Fig. 1) (*7*).

As the study by (*3*) demonstrated, the breakdown of hydrous minerals under warm subduction conditions can occur beneath the forearc mantle, and the expelled free water transforms the overlying mantle peridotite to serpentinite, which can markedly influence its seismic properties. A number of critical geophysical observations in southwest Japan indicate the presence of serpentinized forearc mantle. For example, the forearc mantle in southwest Japan exhibits reduced seismic velocities and high Poisson's ratios, suggesting a high degree of serpentinization (*8*, *9*). Observations of seismic anisotropy from *S*-wave splitting reflect the deformation-induced preferred orientation of serpentinite in the forearc mantle (*10*). Although splitting measurements in the Japan subduction zone generally reveal trench-parallel anisotropy (*11*, *12*), large delay times associated with the splitting measurements in southwest Japan, much greater than those in northeast Japan (Fig. 1) (*13*, *14*), require an antigorite-bearing serpentinite layer with a steep foliation above the slab surface (*15*–*17*). Furthermore, the occurrence of nonvolcanic low-frequency tremors in the leading edge of the mantle wedge at depths of 30 to 40 km in southwest Japan is closely linked to serpentinization-driven fluid overpressure (*18*, *19*). In contrast, a low degree of serpentinization is expected in the forearc mantle in a cold subduction environment, such as that in northeast Japan (*20*).

In this study, we explore the case of the southwest Japan subduction system to clarify a causal relation between warm subduction conditions and serpentinization in the forearc mantle using two-dimensional (2D) numerical models. Unlike previous studies (*21*–*23*), our models predict spontaneous growth of the serpentinite layer, allowing mantle hydration by free water and anisotropic permeability of the serpentinite layer, and constrain the lateral extent of serpentinization and fluid pathways in the serpentinite layer for different thermal conditions. On the basis of our models, we suggest that the anisotropic permeability of the serpentinite layer plays a key role in controlling fluid migration and distribution in the forearc mantle, providing useful insights into the complexities observed in seismic wavefields and the occurrence of deep nonvolcanic tremors in the Japan subduction zone.

RESULTS

Several earlier numerical model studies explored fluid transport in the mantle wedge. The study by (*21*) first considered hydration in the forearc mantle by free water and showed that the breakdown depth of the hydrated mantle incorporated in the deeper mantle wedge is controlled by the thermal conditions of the subducting slab. The study by (*22*) prescribed an a priori serpentinite layer along the slab surface in the forearc mantle and evaluated the role of its anisotropic permeability in the fluid flow toward the corner of the mantle wedge.

Unlike previous studies, our numerical models differ in that we allow spontaneous hydration of the mantle wedge, which generates the serpentinite layer, and fluid flow through the layer is controlled by its anisotropic permeability (see Materials and Methods for details). We conduct 2D finite element model experiments, considering thermal conditions for southwest (warm) and northeast (cold) Japan along the trench-normal profiles (Fig. 1). For comparison, an

[1]Department of Earth System Sciences, Yonsei University, 50 Yonsei-ro Seodaemun-gu, Seoul 03722, Republic of Korea. [2]School of Earth and Environmental Sciences, Seoul National University, 1 Gwanak-ro, Gwanak-gu, Seoul 08826, Republic of Korea.
*Corresponding author. Email: younghkim@snu.ac.kr

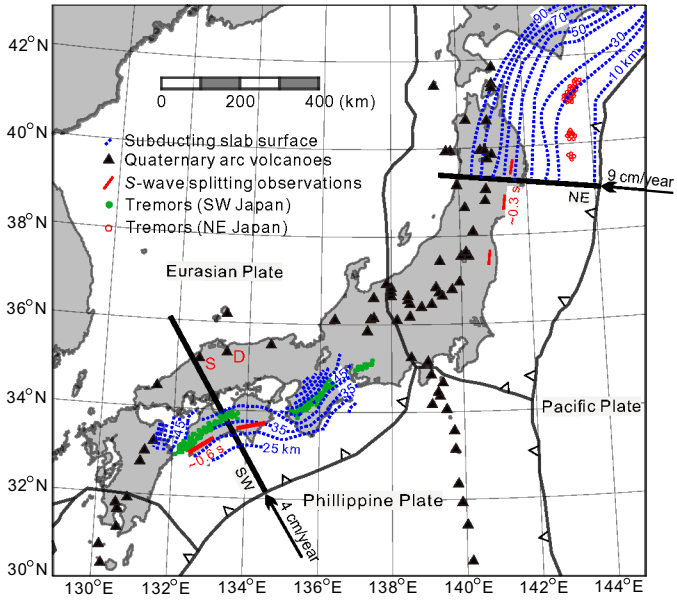

Fig. 1. Seismic and geological probe of the Japan subduction zone. The map shows distributions of Quaternary arc volcanoes (*3*), shear-wave splitting results (*11*, *12*, *14*), and low-frequency nonvolcanic tremors in southwest and northeast Japan (*18*, *36*). The orientations of the red lines correspond to the fast polarization direction, and their lengths correspond to the delay times between the fast and slow *S*-wave arrivals derived from the shear-wave splitting analysis. The modeled profiles are depicted as thick black lines in southwest and northeast Japan. The top interface of the subducting plate is taken from (*19*) and (*36*). S, Sambe; D, Daisen.

intermediate temperature between the warm and cold conditions (denoted as "ordinary") is considered in the subduction experiment using a convergence rate of 6 cm/year and an age of 70 million years (Ma) for the subducting slab. The model subdomains consist of the kinematically subducting slab, deforming mantle wedge and stationary overlying continental crust. The incompressible Stokes and energy equations describe the solid-state flow in the subdomains. The mineral-bound water stored in the hydrated uppermost portion of the subducting slab, consisting of the sediment layer, basaltic oceanic crust, and lithospheric mantle, is injected into the mantle and provides free water to the overlying mantle wedge through dehydration, controlled by the phase diagrams of the water solubilities calculated from the Perple_X program (*24*). The free water percolating through the overlying mantle wedge transforms dry mantle into hydrated mantle including serpentinite and vice versa, controlled by the phase diagram of mantle peridotite. The transports of mineral-bound and free water are governed by solid-state flow and solid-state flow plus Darcy velocity, respectively.

Figure 2 shows near–steady-state temperatures of the hydrated portion of the subducting slab and base of the mantle wedge for depths of 0 to 120 km obtained from the southwest Japan, ordinary, and northeast Japan experiments on the phase diagrams of water solubilities. In the southwest Japan experiment, both the sediment layer and the basaltic oceanic crust are mostly dehydrated beneath the forearc mantle (Fig. 2, A and B), consistent with the transformation of metabasalt to eclogite (*3*). The lithospheric mantle is dehydrated at sub-forearc (~80 km) and subarc depths (~110 km) through breakdown of brucite and serpentine (antigorite), respectively (Fig. 2C). Because the temperatures of the sediment layer and the upper portion of the basaltic oceanic crust are above the solidi of the sedimentary and basaltic rocks (*25*, *26*), slab melting occurs, consistent with the Quaternary arc adakites in the overlying plate (Fig. 1) (*7*). On the other hand, in the ordinary and northeast Japan experiments, only dehydration of the sediment layer and basaltic oceanic crust occurs, consistent with the absence of Quaternary arc adakites in northeast Japan (*27*). No lithospheric mantle is dehydrated beneath the arc, consistent with previous studies (*23*, *28*). Base temperature of the mantle wedge is identical to the slab surface temperature (Fig. 2D). The base temperature indicates that the sub-forearc base of the mantle wedge enables serpentinization in all three experiments when sufficient free water is provided.

In the southwest Japan experiment, the dehydration of both the sediment layer and the basaltic oceanic crust begins before reaching the downdip depth of the slab-mantle decoupling zone (a depth of 75 km) (Fig. 3A), and as a result, a large amount of free water is released to the base of the mantle wedge at this depth (Fig. 3B). Free water from the brucite breakdown in the underlying lithospheric mantle is also incorporated into that from the overlying crust. Because the corner flow above the downdip region is substantially weakened due to slab decoupling from the mantle wedge, little free water is incorporated into the corner flow. Instead, the free water transforms the base of the mantle wedge in the downdip region to serpentinite (Fig. 3, B and C), as the base temperature is sufficiently low enough for serpentinization (Fig. 2D). With time, the free water continuously released from the subducting slab passes through the serpentinite layer at ~10 cm/year, comparable to the estimate (*29*), and spontaneously transforms the shallower base of the mantle wedge to the serpentinite layer toward the corner of the mantle wedge (Fig. 4 and movies S1 and S2). The mean growth rate of the serpentinite layer is approximately 0.33 cm/year, and the layer reaches the corner of the mantle wedge at approximately 24 Ma. The free water expelled at greater depths (>~75-km depth) transforms the base of the mantle wedge to chlorite-bearing lherzolite (no serpentine) (Fig. 2D). The thickness of the hydrated layer is, however, restricted to several kilometers due to the thin cold thermal boundary layer on the slab surface (Fig. 3A). The hydrated base incorporated into the corner flow toward the deeper mantle gradually breaks down with depth (i.e., chlorite breakdown) and provides free water to the overlying mantle wedge. Most of the free water percolating into the mantle wedge transforms the dry mantle into the hydrated mantle (e.g., wet olivine) (Fig. 4). Because the anhydrous mantle can only hold up to 0.15 weight % (wt %) of bound-water (Fig. 2D), most of the water finally reaches the overlying crust; only a small amount of free water is thus incorporated in the corner flow and leaves the model domain (Fig. 4) [e.g., (*23*, *30*)]. The isotropic permeability of the serpentinite layer (no foliated serpentinite) inhibits fluid flow toward the corner of the mantle wedge (see the Supplementary Materials).

Contrary to the results for the warm slab, which show shallow dehydration before reaching downdip depths, the sediment layer and basaltic oceanic crust of both intermediate and cold slabs undergo deeper dehydration, occurring beyond the downdip depth of the decoupling zone (Fig. 2, A and B). No dehydration of the lithospheric mantle occurs in the two experiments (Fig. 2C). Accordingly, the serpentinite layer is absent due to the lack of free water, although the base of the mantle wedge is cold enough for serpentinization. The free water originating from the slab deeper than the downdip

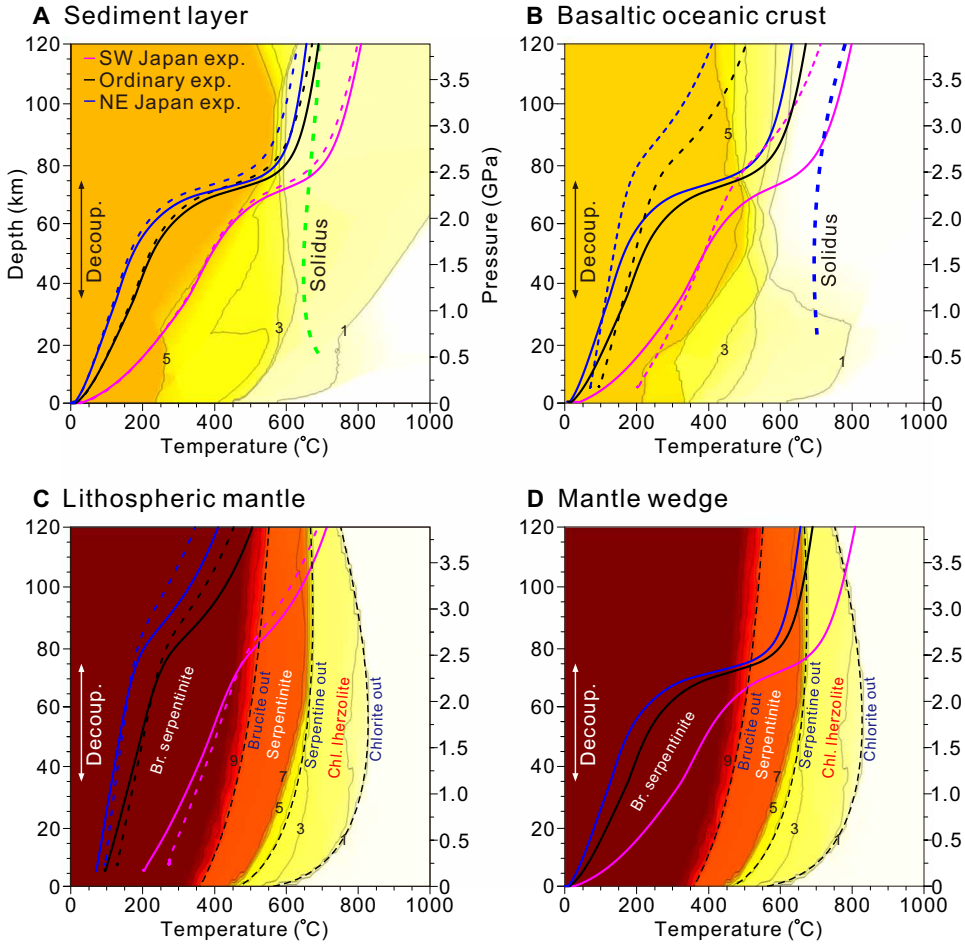

Fig. 2. Numerical modeling results from the southwest Japan, ordinary, and northeast Japan experiments. Geotherms and water solubilities of the sediment layer, basaltic oceanic crust and lithospheric mantle of the subducting slab, and wedge base temperatures and water solubility of the mantle wedge are shown. The numbers indicate water solubilities (wt %). Colored thin solid and dashed lines represent pressure-temperature (*P-T*) conditions of the top and bottom interfaces of each layer, respectively. The double arrow indicates the range of the decoupling zone. (**A**) Geotherms in the sediment layer. The green thick dashed line indicates the wet sediment solidus (*25*). (**B**) Geotherms in the basaltic oceanic crust. The blue thick dashed line indicates the wet basalt solidus (*26*). (**C**) Geotherms in the hydrated lithospheric mantle. Br. serpentinite, brucite-bearing serpentinite; Serpentinite, serpentinite without brucite; Chl. Lherzolite, chlorite-bearing lherzolite. The thin dashed lines represent brucite-, serpentine-, and chlorite-out phase boundaries, respectively. (**D**) Wedge base temperatures on the water solubility of the mantle wedge. The solid lines indicate wedge base temperatures identical to slab surface temperatures.

depth transforms the base of the mantle wedge (chlorite-bearing lherzolite) above the fully coupled slab-mantle interface. The base is incorporated into the corner flow and gradually breaks down with depth [e.g., (*23*, *30*)]. Model results considering diverse subduction parameters and conditions show that the spontaneous growth of the serpentinite layer toward the corner of the mantle wedge can be observed only when we incorporate the anisotropic permeability of the serpentinite layer for the warm slab (see the Supplementary Materials).

DISCUSSION

Our numerical models show that shallow dehydration of a warm slab generates serpentinite in the downdip region of the decoupling zone, and this layer extends updip toward the corner of the mantle wedge through spontaneous hydration by free water flow along the serpentinite foliation. The generation of the serpentinite layer and the fluid flow regulated by its anisotropic permeability support strong anisotropy in the forearc mantle wedge and nonvolcanic tremors at its corner, as observed in southwest Japan. The trench-parallel fast *S*-wave polarization direction and associated large delay time of approximately 0.6 s (*11*, *12*) require a serpentinite layer in addition to B-type olivine fabric (*16*). We note that even larger delay times (~1.0 s) observed in Ryukyu (*16*) can be explained by shallower Moho depth (~25 km) than that (~35 km) in southwest Japan, which allows a larger extent of the serpentinite layer toward the corner of the mantle wedge. The occurrence of nonvolcanic tremors (*19*) and an anomalously high Poisson's ratio (*8*, *9*) further indicate elevated fluid overpressure in the serpentinite layer (*18*).

In addition to the updip fluid migration for tremor generation (*18*, *29*), there are other mechanisms under the warm subduction environment based on geological and numerical studies, which are brittle thrusting at near-lithostatic fluid overpressure within viscous shear zone (*31*, *32*) and in situ dehydration reactions for the high fluid pressure (*33*). The implication from our model results is that

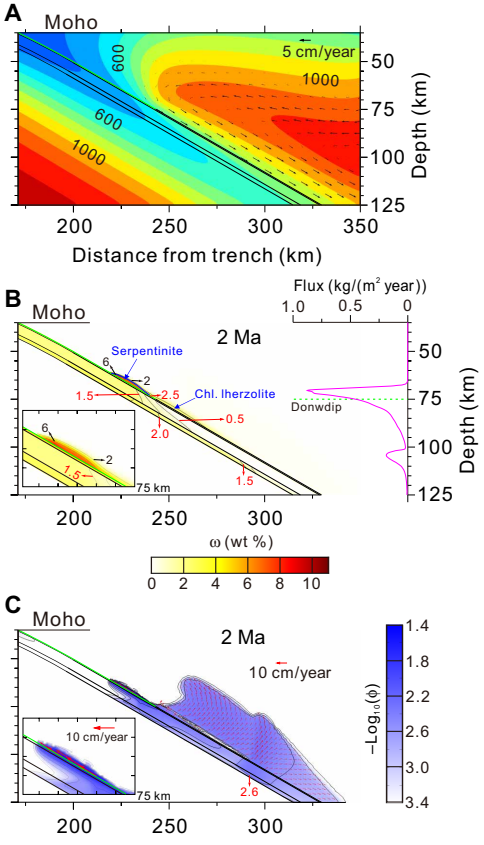

Fig. 3. Distributions of temperature and velocity, mineral-bound water, and free water with velocity from the southwest Japan experiment. (**A**) Distributions of temperature depicted every 100°C and velocity (cm/year). Black solid lines represent boundaries of the sediment layer, basaltic oceanic crust, and lithospheric mantle. The decoupling zone prescribed on the top of the sediment layer is depicted by the green line. The velocity is proportional to the reference scale of 5 cm/year. (**B**) Distributions of mineral-bound water and free water flux from the subducting slab at 2 Ma after the free water releases. Black and red arrows with numbers indicate contour values of bound water in the mantle wedge (every 2 wt %) and subducting slab (every 0.5 wt %), respectively. (**C**) Distribution of free water with its velocity at 2 Ma after the free water releases. The red arrow with a number indicates a contour value of free water. Volume fractions of free water less than 0.0004 (3.4 on the log scale) are not shown. The velocity is proportional to the reference scale of 10 cm/year.

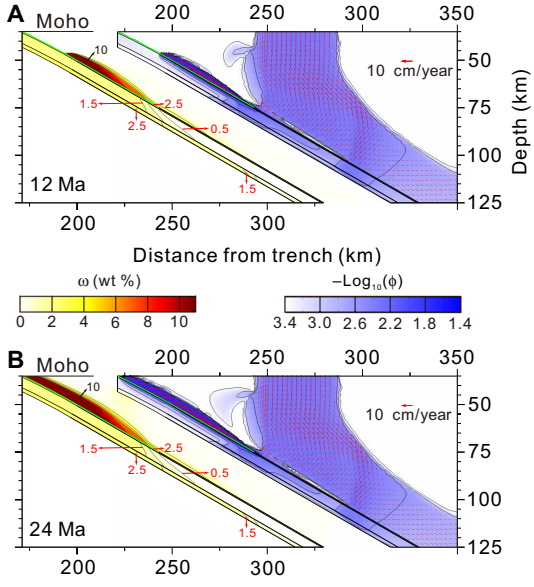

Fig. 4. Distributions of mineral-bound water and free water in the mantle wedge and the subducting slab obtained from the southwest Japan experiment. Distributions of mineral-bound water and free water obtained at 12 Ma (**A**) and 24 Ma (**B**) after free water release are shown. Other notations are the same, as those shown in Fig. 3.

the upward migration of fluids from the descending slab promotes hydration locally at the plate interface, which becomes weak in terms of frictional coupling. The hydrated plate interface has the potential to generate tremors, and these events are mainly located in the leading edge of the mantle wedge at depths of 30 to 40 km in southwest Japan, resulting from the buildup of pore pressure. The wide distribution of high $^{3}He/^{4}He$ values and associated ^{20}Ne and Cl^{-} concentrations from the Kii Peninsula, southwest Japan, also supports the updip fluid migration driven by the dehydration of the descending slab (*34*).

Our models under intermediate and cold slab conditions, on the other hand, show hydrated mantle above the fully coupled slab-mantle interface, which is incorporated into the corner flow of the mantle wedge. The absence of the serpentinite layer in the models supports a number of geophysical observations in northeast Japan, such as the small delay times of shear-wave splitting (~0.3 s) (*12*, *14*), the paucity of deep nonvolcanic tremors, and the cold and dry nature of the forearc mantle (Fig. 1) (*20*, *35*). The study by (*36*) reported the occurrence of shallow low-frequency nonvolcanic tremors at 10- to 25-km depths on the plate interface, implying no subarc serpentinite layer. In addition, the hydrated base of the mantle wedge observed in the northeast Japan experiment is consistent with the extent of the low-velocity zone atop the subducting slab at depths of 80 to 130 km in northeast Japan (*37*).

Because our numerical models do not consider compaction pressure and the dynamic response of the overlying crust, the bifurcation of the free water toward the tip of the mantle wedge and the subarc mantle (*38*) does not occur. If bifurcation occurs, the free water percolating toward the corner of the mantle wedge may further hydrate the base of the forearc mantle. Also, there are expected feedbacks between volume expansion of the serpentinite phases and their hydrodynamic properties such as permeability and porosity, which are not constrained in our study. We consider only the near–steady-state solid-state flow and mineral-bound water distributions in the subducting slab, in contrast to the time-evolving subduction of the hot Shikoku basin initiated along Shikoku Island at approximately 17 Ma (*39*). If time-evolving subduction is considered, even shallower dehydration of the subducting slab may provide free water to the corner of the mantle wedge and result in still faster growth of the serpentinite layer than that (~24 Ma) observed in our model calculations. In addition, the self-consistent slab decoupling may occur if the low-viscosity serpentinite layer is established at the base of the forearc mantle wedge, which mechanically decouples the subducting slab from the overlying mantle wedge (*40*). Thus, time-evolving subduction with mechanical response of the serpentinite may be required for the self-consistent development of the serpentinite layer in the forearc mantle.

Although our model experiments show that warm subduction conditions explain the observed strong seismic anisotropy and the

occurrence of nonvolcanic tremors in southwest Japan, applications to other subduction zones should be conducted with caution. In Cascadia, the forearc region shows a trench-normal fast direction of shear-wave splitting (*41*), in contrast to the expected trench-parallel fast direction produced by the serpentinite layer. The strong trench-normal corner flow driven by slab-driven toroidal flow may overshadow the trench-parallel anisotropy in the serpentinite layer. In Hikurangi, the occurrence of nonvolcanic tremors in the forearc mantle is closely linked to fluid overpressure along the slab interface (*42*), although the old subducting Pacific plate (~120 Ma) may not yield a serpentinite layer in the forearc mantle. However, shallow dehydration resulting in the serpentinite layer in the forearc mantle may be possible if great frictional heating occurs by strong coupling along the plate interface (*43*) due to the trenchward migration of the overlying Australian plate and/or the subduction of the buoyant thick Hikurangi Plateau (*44*).

MATERIALS AND METHODS

Governing equations

In our model calculations, the solid-state flow of the mantle wedge is calculated using the incompressible Stokes and energy equations. The energy equation is calculated by using only the prescribed convergence rate for the kinematically driven subducting slab and a zero-migration rate for the stationary overlying continental crust. The governing equations and rheology are succinctly described here, and the readers may refer to the previous studies (*23*, *30*) for detailed information. The incompressible Stokes and energy equations can be described as follows

$$0 = \nabla \cdot \vec{V}_s \tag{1}$$

continuity equation,

$$0 = -\nabla P + \nabla \cdot (2\eta \dot{\varepsilon}) \tag{2}$$

momentum equation,

$$\rho_s C_p \left(\frac{\partial T}{\partial t} + \vec{V}_s \cdot \nabla T \right) = \nabla \cdot (k \nabla T) + H \tag{3}$$

energy equation, where $\vec{V}_s$ is the solid velocity, P is the dynamic pressure, η is the shear viscosity, $\dot{\varepsilon}$ is the strain rate tensor, ρ_s is the solid density, C_p is the specific heat, T is the temperature, t is the time, k is the thermal conductivity, and H is the radiogenic heat production. The net mantle adiabat ($\overline{T}$) is added to the calculated temperatures as a posterior.

Although the mantle viscosity may be expressed as the composite viscosity of the diffusion and dislocation creep, the thermal and flow structures of the kinematically driven mantle wedge can be calculated by the diffusion creep rheology of wet olivine (*45*) with little loss of accuracy (*46*), defined as follows

$$\eta = \frac{\mu}{2A} \left(\frac{b}{d} \right)^{-m} \exp\left(\frac{E + PV}{R(T + \overline{T})} \right) \tag{4}$$

mantle viscosity, where μ is the shear modulus; A is the pre-exponent factor; b is the Burgers vector; d is the grain size; m is the grain size exponent; E and V are the activation energy and volume, respectively; and R is the gas constant.

The solid flow of the mineral-bound water is governed by the solid-state flow of the subducting slab and mantle wedge, while the fluid flow of the free water is governed by the solid-state flow plus Darcy velocity driven by the density difference between the solid and free water. Using the small-porosity approximation and zero-compaction approximation (*23*, *47*), the mass conservation of the mineral-bound water and free water can be calculated by the following equations:

$$\frac{\partial \omega}{\partial t} + \nabla \cdot (\vec{V}_s \omega) = \Gamma_{f \longrightarrow s} / \rho_s + \nabla \cdot (\kappa_\omega \nabla \omega) \tag{5}$$

mass conservation of mineral-bound water,

$$\frac{\partial \phi}{\partial t} + \nabla \cdot (\vec{V}_f \phi) = \Gamma_{s \longrightarrow f} / \rho_f + \nabla \cdot (\kappa_\phi \nabla \phi) \tag{6}$$

mass conservation of free water, where ω and ϕ are the mass and volume fractions of mineral-bound water and free water ($\cdot$), $\vec{V}_s$ and $\vec{V}_f$ are the solid and free water velocities, $\Gamma_{f \longrightarrow s}$ and $\Gamma_{s \longrightarrow f}$ are the rates of mass transfer by hydration and dehydration, ρ_s and ρ_f are the solid and free water densities, and κ_ω and κ_ϕ are the artificial diffusivities of mineral-bound water and free water, respectively. The diffusion terms $\nabla \cdot (\kappa_\omega \nabla \omega)$ and $\nabla \cdot (\kappa_\phi \nabla \phi)$ are added to improve model stability [e.g., (*23*, *30*, *47*)].

The fluid flow of free water in the model domain is calculated by neglecting the dynamic pressure term [e.g., (*23*, *48*)], shown as follows

$$\vec{V}_f = \vec{V}_s - \frac{K}{\eta_f \phi} (\rho_s - \rho_f) \vec{g} \tag{7}$$

free water velocity, where K is the permeability, η_f is the free water viscosity, and $\vec{g}$ is the gravitational acceleration. The permeability can be approximated as follows

$$K = \frac{d^2 \phi^3}{C_d} \tag{8}$$

permeability, where C_d is the geometrical factor. Laboratory experiments suggest that the serpentinite permeability is lower than that of the mantle peridotite, while the permeability along the serpentinite foliation is approximately two orders of magnitude higher than that normal to the foliation (*29*). Thus, the experiments suggest that the serpentinite layer develops along the slab surface toward the corner of the mantle wedge because the fluid flows along the foliation parallel to the slab surface. To consider the anisotropic permeability of the serpentinite layer, we assume that the foliation in the serpentinite layer is parallel to the slab surface and that the permeabilities normal to and parallel to the slab surface (K_n and K_p) are 0.002 K and 0.1 K, respectively, where K is the calculated isotropic mantle permeability in Eq. 8 [e.g., (*22*, *49*)]. As serpentinite is generated at the base of the mantle wedge, a large shear strain localized in the mechanically weak serpentinite can lead to the development of foliation, and the resultant serpentinite foliation provides a fluid pathway for free water. We assume that the anisotropic permeability of the serpentinite layer due to foliation is activated when 25% of the mantle peridotite at the base of the mantle wedge is transformed to serpentinite. Regardless of the activation condition, the hydrated base can hold mineral-bound water up to 10.86 wt %, which is the maximum water solubility of mantle peridotite.

Laboratory experiments show rapid (de)hydration of the mantle peridotite without long-term persisting metastable phases (*50*), and we assume that all phase transformations are completed over the

dehydration length (l). The mass transfer from free water to mineral-bound water by hydration is calculated by using the following simplified kinematic relation as [e.g., (*23*, *30*)]

$$\Gamma_{f\longrightarrow s} = \frac{\rho_s \,|\, \vec{V}_s \,|\, (\omega_{\max(P,T+\overline{T})} - \omega_{(P,T+\overline{T})})}{l} \quad (9)$$

rate of mass transfer from free water to mineral-bound water, where $|\,\vec{V}_s\,|$ is the magnitude of the solid velocity, $\omega_{\max(P,T+\overline{T})}$ is the maximum water solubility of the solid at the given pressure and temperature, and $\omega_{(P,T+\overline{T})}$ is the mass fraction of mineral-bound water in the solid. The mass transfer from mineral-bound water to free water ($\Gamma_{s\longrightarrow f}$) is defined by adding the negative sign to $\Gamma_{f\longrightarrow s}$. No rehydration is considered in the subducting slab, but both dehydration and hydration are considered in the mantle wedge [e.g., (*23*, *30*)]. The values used in our numerical models are specified in table S1.

Model setup and numerical method

Since the subducting slab geometries do not vary significantly along southwest and northeast Japan, we consider 2D trench-normal cross sections of the subduction zones (Fig. 1 and fig. S1) [e.g., (*3*)]. Because we focus on the effects of the convergence rate and age of the subducting slab on the seismological characteristics in the forearc region, both subduction zones are simplified using the same model geometry, which is 350 km long and 125 km deep (fig. S1). The subducting slab and overlying continental crust have thicknesses of 100 and 35 km, respectively (*51*). The convergence rates and ages of the subducting slabs in southwest and northeast Japan are approximately 4 cm/year and 15 Ma and 9 cm/year and 130 Ma, respectively. The radiogenic heat productions of the oceanic crust, continental crust, and mantle are obtained from the values of tholeiitic basalt, granite (half value), and peridotite (*52*). For the boundary conditions of the solid-state flow, the slab-mantle decoupling zone on the slab surface is prescribed with 5% of the convergence rate for depths from 35 to 70 km, including the linear velocity ramp at a depth of 75 km, consistent with low heat flows of the forearc regions observed in southwest and northeast Japan (*53*). Below the downdip depth of the decoupling zone at a depth of 75 km, full coupling is applied to the slab surface [e.g., (*23*, *30*, *54*)]. No-slip and open boundary conditions are prescribed on the continental Moho and outer boundaries of the mantle wedge, respectively. For the temperature boundary condition, the half-space cooling models are calculated using a mantle potential temperature of 1350°C. The calculated temperature profiles for the relevant slab ages and 50 Ma are prescribed on the trench side and the back-arc side boundaries, respectively. The net mantle adiabat is added to the calculated temperatures as a posterior. The bottom of the subducting slab is insulated, and the horizontal boundary of the subducting slab at a depth of 125 km is open. The top surface of the model domain is fixed at 0°C.

The amount and depth-extent of the mineral-bound water in the subducting slab typically show large spatial and temporal variations with varying lithology and structure (*55*–*57*). For simplicity, we construct our model such that the hydrated portion of the subducting slab consists of a sediment layer (1 km thick), basaltic oceanic crust (5 km thick), and lithospheric mantle (2 km thick) (fig. S1B) [e.g., (*23*, *28*)]. The Antilles terrigenous, mid-ocean ridge basalt (MORB) and depleted MORB mantle (DMM) compositions are used for the three layers from the top to the bottom [(*55*) and table S2]. The water solubilities of the three lithologies are calculated using the Perple_X program (ver. 6.8.6) (*24*) by simplifying the bulk compositions as the Na_2O-CaO-K_2O-MgO-FeO-MnO-Al_2O_3-TiO_2-SiO_2-H_2O-CO_2 system [e.g., (*55*)]. The activity models used in the Perple_X program are described in table S3. To consider the depth-dependent and localized distribution of mineral-bound water in the subducting slab [e.g., (*23*, *30*, *54*)), 100%, 40%, and 25% hydrations of the three layers are assumed. This indicates that the sediment layer is fully hydrated but the basaltic oceanic crust and underlying lithospheric mantle are partially hydrated; the partial hydration represents the fully hydrated zone (e.g., fault and fracture zones) surrounded by ambient anhydrous (dry) zone (*56*, *58*). Thus, the dehydration of the fully hydrated zones in the basaltic oceanic crust and lithospheric mantle is controlled by their water solubilities, but the amounts of the expelled free water are reduced to 40 and 25%, respectively, compared with those from the fully hydrated layers [e.g., (*23*)]. The same water solubility of the DMM composition is used for that of the mantle wedge with the initial bound-water of 10^{-4} (0.01 wt %).

The relevant values of mineral-bound water are prescribed on the trench side boundary of the layers. A background mass fraction of 10^{-4} (0.01 wt %) is prescribed on the outer boundaries of the mantle wedge for the back-arc mantle (*59*). No bound-water flux boundaries are prescribed on the other inner and outer boundaries to prevent the artificial diffusion of the mineral-bound water across the layers, mantle wedge, and overlying continental crust [e.g., (*23*, *30*)]. For the fluid flow of free water, no free water flux boundary is prescribed on the bottom of the hydrated portion of the subducting slab, and a background volume fraction of free water (10^{-4}) is prescribed on the other open boundaries (fig. S1C). The whole model domain consists of 65,348 unstructured triangular elements with sizes ranging from 0.1 to 2 km. Mesh refinements are applied to the hydrated portion of the subducting slab and the bases of the mantle wedge and the overlying continental crust using element sizes ranging from 0.1 to 0.625 km to improve the accuracy of the model calculations.

The governing equations with the defined rheologies and water solubilities are simultaneously calculated using the commercial finite element package COMSOL Multiphysics (ver. 5.5). After the near–steady-state distributions of the temperature and velocity and the water contents in the hydrated portion of the subducting slab are obtained for a runtime of 270 Ma, the free water is released for 28 Ma. To stabilize the model calculations, the standard streamline and crosswind diffusions are used for the Stokes equations, and further stabilization of the isotropic diffusion is used for both the solid and fluid flow equations of mineral-bound and free water [e.g., (*23*, *30*, *54*)]. The segregated solver with the multifrontal massively parallel sparse direction solver (MUMPS) is used with the generalized-alpha method for time stepping.

SUPPLEMENTARY MATERIALS

Supplementary material for this article is available at http://advances.sciencemag.org/cgi/content/full/7/28/eabf8934/DC1

REFERENCES AND NOTES

1. A. Hasegawa, J. Nakajima, Seismic imaging of slab metamorphism and genesis of intermediate-depth intraslab earthquakes. *Prog. Earth Planet. Sci.* **4**, 12 (2017).
2. D. A. Wiens, J. A. Conder, U. H. Faul, The seismic structure and dynamics of the mantle wedge. *Annu. Rev. Earth Planet. Sci.* **36**, 421–455 (2008).
3. S. M. Peacock, K. Wang, Seismic consequences of warm versus cool subduction metamorphism: Examples from southwest and northeast Japan. *Science* **286**, 937–939 (1999).
4. Y. Fukao, S. Hori, M. Ukawa, A seismological constraint on the depth of basalt–eclogite transition in a subducting oceanic crust. *Nature* **303**, 413–415 (1983).

5. A. Kato, T. Iidaka, R. Ikuta, Y. Yoshida, K. Katsumata, T. Iwasaki, S. i. Sakai, C. Thurber, N. Tsumura, K. Yamaoka, T. Watanabe, T. Kunitomo, F. Yamazaki, M. Okubo, S. Suzuki, N. Hirata, Variations of fluid pressure within the subducting oceanic crust and slow earthquakes. *Geophys. Res. Lett.* **37**, L14310 (2010).
6. J. Wang, D. Zhao, P wave anisotropic tomography of the Nankai subduction zone in Southwest Japan. *Geochem. Geophys. Geosyst.* **13**, Q05017 (2012).
7. P. A. Morris, Slab melting as an explanation of Quaternary volcanism and aseismicity in southwest Japan. *Geology* **23**, 395–398 (1995).
8. X. Liu, D. Zhao, S. Li, Seismic imaging of the Southwest Japan arc from the Nankai trough to the Japan Sea. *Phys. Earth Planet. In.* **216**, 59–73 (2013).
9. S. Xia, D. Zhao, X. Qiu, Tomographic evidence for the subducting oceanic crust and forearc mantle serpentinization under Kyushu, Japan. *Tectonophysics* **449**, 85–96 (2008).
10. M. D. Long, P. G. Silver, The subduction zone flow field from seismic anisotropy: A global view. *Science* **319**, 315–318 (2008).
11. M. K. Salah, T. Seno, T. Iidaka, Upper mantle anisotropy beneath central and southwest Japan: An insight into subduction-induced mantle flow. *J. Geodyn.* **46**, 21–37 (2008).
12. E. Wirth, M. D. Long, Frequency-dependent shear wave splitting beneath the Japan and Izu-Bonin subduction zones. *Phys. Earth Planet. In.* **181**, 141–154 (2010).
13. Z. Huang, D. Zhao, L. Wang, Shear wave anisotropy in the crust, mantle wedge, and subducting Pacific slab under northeast Japan. *Geochem. Geophys. Geosyst.* **12**, Q01002 (2011).
14. J. Nakajima, A. Hasegawa, Shear-wave polarization anisotropy and subduction-induced flow in the mantle wedge of northeastern Japan. *Earth Planet. Sci. Lett.* **225**, 365–377 (2004).
15. S. J. Brownlee, B. R. Hacker, G. E. Harlow, G. Seward, Seismic signatures of a hydrated mantle wedge from antigorite crystal-preferred orientation (CPO). *Earth Planet. Sci. Lett.* **375**, 395–407 (2013).
16. I. Katayama, K. Hirauchi, K. Michibayashi, J. Ando, Trench-parallel anisotropy produced by serpentine deformation in the hydrated mantle wedge. *Nature* **461**, 1114–1117 (2009).
17. M. Mookherjee, G. C. Capitani, Trench parallel anisotropy and large delay times: Elasticity and anisotropy of antigorite at high pressures. *Geophys. Res. Lett.* **38**, L09315 (2011).
18. I. Katayama, T. Terada, K. Okazaki, W. Tanikawa, Episodic tremor and slow slip potentially linked to permeability contrasts at the Moho. *Nat. Geosci.* **5**, 731–734 (2012).
19. K. Obara, Nonvolcanic deep tremor associated with subduction in southwest Japan. *Science* **296**, 1679–1681 (2002).
20. G. A. Abers, P. E. van Keken, B. R. Hacker, The cold and relatively dry nature of mantle forearcs in subduction zones. *Nat. Geosci.* **10**, 333–337 (2017).
21. H. Iwamori, Transportation of H_2O and melting in subduction zones. *Earth Planet. Sci. Lett.* **160**, 65–80 (1998).
22. M. Morishige, P. E. van Keken, Along-arc variation in short-term slow slip events caused by 3-D fluid migration in subduction zones. *J. Geophys. Res. Solid Earth* **122**, 1434–1448 (2017).
23. C. Lee, D. Seoung, N. G. Cerpa, Effect of water solubilities on dehydration and hydration in subduction zones and water transport to the deep mantle: Implications for natural subduction zones. *Gondw. Res.* **89**, 287–305 (2021).
24. J. A. D. Connolly, Computation of phase equilibria by linear programming: A tool for geodynamic modeling and its application to subduction zone decarbonation. *Earth Planet. Sci. Lett.* **236**, 524–541 (2005).
25. G. T. Nichols, P. J. Wyllie, C. R. Stern, Subduction zone melting of pelagic sediments constrained by melting experiments. *Nature* **371**, 785–788 (1994).
26. M. W. Schmidt, S. Poli, Experimentally based water budgets for dehydrating slabs and consequences for arc magma generation. *Earth Planet. Sci. Lett.* **163**, 361–379 (1998).
27. J.-I. Kimura, T. Yoshida, Contributions of slab fluid, mantle wedge and crust to the origin of Quaternary lavas in the NE Japan arc. *J. Petrol.* **47**, 2185–2232 (2006).
28. P. E. van Keken, B. R. Hacker, E. M. Syracuse, G. A. Abers, Subduction factory: 4. Depth-dependent flux of H_2O from subducting slabs worldwide. *J. Geophys. Res.* **116**, B01401 (2011).
29. S. Kawano, I. Katayama, K. Okazaki, Permeability anisotropy of serpentinite and fluid pathways in a subduction zone. *Geology* **39**, 939–942 (2011).
30. S. Yoo, C. Lee, Correlation of Quaternary volcano clusters with partial melting of mantle wedge, Northeast Japan: A numerical model study. *Geophys. Res. Lett.* **47**, e2019GL086205 (2020).
31. W. M. Behr, A. J. Kotowski, K. T. Ashley, Dehydration-induced rheological heterogeneity and the deep tremor source in warm subduction zones. *Geology* **46**, 475–478 (2018).
32. K. Ujiie, H. Saishu, Å. Fagereng, N. Nishiyama, M. Otsubo, H. Masuyama, H. Kagi, An explanation of episodic tremor and slow slip constrained by crack-seal veins and viscous shear in subduction mélange. *Geophys. Res. Lett.* **45**, 5371–5379 (2018).
33. C. B. Condit, V. E. Guevara, J. R. Delph, M. E. French, Slab dehydration in warm subduction zones at depths of episodic slip and tremor. *Earth Planet. Sci. Lett.* **552**, 116601 (2020).
34. N. Morikawa, K. Kazahaya, M. Takahashi, A. Inamura, H. A. Takahashi, M. Yasuhara, M. Ohwada, T. Sato, A. Nakama, H. Handa, H. Sumino, K. Nagao, Widespread distribution of ascending fluids transporting mantle helium in the fore-arc region and their upwelling processes: Noble gas and major element composition of deep groundwater in the Kii Peninsula, southwest Japan. *Geochim. Cosmochim. Acta* **182**, 173–196 (2016).
35. Z. Yu, D. Zhao, Seismic evidence for water transportation in the forearc off Northern Japan. *J. Geophys. Res. Solid Earth* **125**, e2019JB018600 (2020).
36. S. Tanaka, T. Matsuzawa, Y. Asano, Shallow low-frequency tremor in the Northern Japan trench subduction zone. *Geophys. Res. Lett.* **46**, 5217–5224 (2019).
37. H. Kawakatsu, S. Watada, Seismic evidence for deep-water transportation in the mantle. *Science* **316**, 1468–1471 (2007).
38. H. Wang, R. S. Huismans, S. Rondenay, Water migration in the subduction mantle wedge: A two-phase flow approach. *J. Geophys. Res. Solid Earth* **124**, 9208–9225 (2019).
39. J.-I. Kimura, R. J. Stern, T. Yoshida, Reinitiation of subduction and magmatic responses in SW Japan during Neogene time. *Geol. Soc. Am. Bull.* **117**, 969–986 (2005).
40. B. Reynard, Serpentine in active subduction zones. *Lithos* **178**, 171–185 (2013).
41. M. D. Long, E. A. Wirth, Mantle flow in subduction systems: The mantle wedge flow field and implications for wedge processes. *J. Geophys. Res. Solid Earth* **118**, 583–606 (2013).
42. P. Audet, Y. Kim, Teleseismic constraints on the geological environment of deep episodic slow earthquakes in subduction zone forearcs: A review. *Tectonophysics* **670**, 1–15 (2016).
43. S. Yabe, S. Ide, S. Yoshioka, Along-strike variations in temperature and tectonic tremor activity along the Hikurangi subduction zone, New Zealand. *Earth Planets Space* **66**, 142 (2014).
44. L. M. Wallace, J. Beavan, R. McCaffrey, D. Darby, Subduction zone coupling and tectonic block rotations in the North Island, New Zealand. *J. Geophys. Res.* **109**, B12406 (2004).
45. S.-I. Karato, P. Wu, Rheology of the upper mantle: A synthesis. *Science* **260**, 771–778 (1993).
46. C. Lee, S. D. King, Effect of mantle compressibility on the thermal and flow structures of the subduction zones. *Geochem. Geophys. Geosyst.* **10**, Q01006 (2009).
47. C. R. Wilson, M. Spiegelman, P. E. van Keken, B. R. Hacker, Fluid flow in subduction zones: The role of solid rheology and compaction pressure. *Earth Planet. Sci. Lett.* **401**, 261–274 (2014).
48. N. G. Cerpa, I. Wada, C. R. Wilson, Fluid migration in the mantle wedge: Influence of mineral grain size and mantle compaction. *J. Geophys. Res. Solid Earth* **122**, 6247–6268 (2017).
49. J. Taylor-West, R. F. Katz, Melt-preferred orientation, anisotropic permeability and melt-band formation in a deforming, partially molten aggregate. *Geophys. J. Int.* **203**, 1253–1262 (2015).
50. B. Malvoisin, F. Brunet, Water diffusion-transport in a synthetic dunite: Consequences for oceanic peridotite serpentinization. *Earth Planet. Sci. Lett.* **403**, 263–272 (2014).
51. T. Yamamoto, N. Hoang, Synchronous Japan Sea opening Miocene fore-arc volcanism in the Abukuma Mountains, NE Japan: An advancing hot asthenosphere flow versus Pacific slab melting. *Lithos* **112**, 575–590 (2009).
52. C. Clauser, Radiogenic heat production of rocks, *in Encyclopedia of Solid Earth Geophysics*, H. K. Gupta, Ed. (Encyclopedia of Earth Sciences Series, Springer, 2011).
53. I. Wada, K. Wang, Common depth of slab-mantle decoupling: Reconciling diversity and uniformity of subduction zones. *Geochem. Geophys. Geosyst.* **10**, Q10009 (2009).
54. I. Wada, M. D. Behn, Focusing of upward fluid migration beneath volcanic arcs: Effect of mineral grain size variation in the mantle wedge. *Geochem. Geophys. Geosyst.* **16**, 3905–3923 (2015).
55. B. R. Hacker, H_2O subduction beyond arcs. *Geochem. Geophys. Geosyst.* **9**, Q03001 (2008).
56. I. Grevemeyer, C. R. Ranero, M. Ivandic, Structure of oceanic crust and serpentinization at subduction trenches. *Geosphere* **14**, 395–418 (2018).
57. S. Naif, K. Key, S. Constable, R. L. Evans, Water-rich bending faults at the Middle America Trench. *Geochem. Geophys. Geosyst.* **16**, 2582–2597 (2015).
58. I. Wada, M. D. Behn, A. M. Shaw, Effects of heterogeneous hydration in the incoming plate, slab rehydration, and mantle wedge hydration on slab-derived H_2O flux in subduction zones. *Earth Planet. Sci. Lett.* **353-354**, 60–71 (2012).
59. K. A. Kelley, T. Plank, T. L. Grove, E. M. Stolper, S. Newman, E. Hauri, Mantle melting as a function of water content beneath back-arc basins. *J. Geophys. Res. Solid Earth* **111**, B09208 (2006).
60. T. Ishii, H. Kojitani, M. Akaogi, Phase relations of harzburgite and MORB up to the uppermost lower mantle conditions: Precise comparison with pyrolite by multisample cell high-pressure experiments with implication to dynamics of subducted slabs. *J. Geophys. Res. Solid Earth* **124**, 3491–3507 (2019).

Acknowledgments: We thank K. Hodges, K. Furlong, R. Huismans, and an anonymous reviewer for the careful and constructive suggestions. **Funding:** C.L. acknowledges support from the National Research Foundation of Korea (2017R1A6A1A07015374 and 2019R1A2C1002517) and the Yonsei University Research Fund (2019-22-0010). Y.K. acknowledges support from the Creative Pioneering Researchers Program of Seoul National

University (SNU SRnD 3345-20160014) and the National Research Foundation of Korea (NRF-2019R1G1A1094833). **Author contributions:** C.L. conceptualized the project, conducted numerical modeling, interpreted the results, and wrote the manuscript. Y.K. enhanced the project, interpreted the results, and wrote the manuscript. **Competing interests:** The authors declare that they have no competing interests. **Data and materials availability:** All data needed to evaluate the conclusions in the paper are present in the paper and the Supplementary Materials. Additional data related to this paper may be requested from the authors.

Submitted 26 November 2020
Accepted 27 May 2021
Published 9 July 2021
10.1126/sciadv.abf8934

Citation: C. Lee, Y. Kim, Role of warm subduction in the seismological properties of the forearc mantle: An example from southwest Japan. *Sci. Adv.* **7**, eabf8934 (2021).

Science Advances

Role of warm subduction in the seismological properties of the forearc mantle: An example from southwest Japan

Changyeol Lee and YoungHee Kim

Sci Adv **7** (28), eabf8934.
DOI: 10.1126/sciadv.abf8934